UC Riverside
UC Riverside Previously Published Works

Title

Marangoni force-driven manipulation of photothermally-induced microbubbles.

Permalink

https://escholarship.org/uc/item/10m6w6z5

Journal

Optics Express, 26(6)

ISSN

1094-4087

Authors

Ortega-Mendoza, JG

Sarabia-Alonso, JA

Zaca-Morán, P

et al.

Publication Date

2018-03-19

DOI

10.1364/oe.26.006653

Copyright Information

Peer reviewed

Marangoni force-driven manipulation of photothermally-induced microbubbles

J. G. Ortega-Mendoza,[1,*] J. A. Sarabia-Alonso,[1,2] P. Zaca-Morán,[3] A. Padilla-Vivanco,[1] C. Toxqui-Quitl,[1] I. Rivas-Cambero,[1] J. Ramirez-Ramirez,[2] S. A. Torres-Hurtado,[2] and R. Ramos-García[2]

[1]División de Ingenierías, Universidad Politécnica de Tulancingo, CP 43629, Hidalgo, Mexico
[2]Departamento de Óptica, Instituto Nacional de Astrofísica, Óptica y Electrónica, CP 72840, Puebla, Mexico
[3]Instituto de Ciencias, Benemérita Universidad Autónoma de Puebla, CP 72050, Puebla, Mexico
[*]jose.ortega@upt.edu.mx

Abstract: The generation and manipulation of microbubbles by means of temperature gradients induced by low power laser radiation is presented. A laser beam (λ = 1064 nm) is divided into two equal parts and coupled to two multimode optical fibers. The opposite ends of each fiber are aligned and separated a distance D within an ethanol solution. Previously, silver nanoparticles were photo deposited on the optical fibers ends. Light absorption at the nanoparticles produces a thermal gradient capable of generating a microbubble at the optical fibers end in non-absorbent liquids. The theoretical and experimental studies carried out showed that by switching the thermal gradients, it is possible to generate forces in opposite directions, causing the migration of microbubbles from one fiber optic tip to another. Marangoni force induced by surface tension gradients in the bubble wall is the driving force behind the manipulation of microbubbles. We estimated a maximum Marangoni force of 400 nN for a microbubble with a radius of 110 μm.

OCIS codes: (140.7010) Laser trapping; (140.6810) Thermal effects; (060.2310) Fiber optics; (160.4236) Nanomaterials.

References and links

1. A. Hashmi, G. Yu, M. Reilly-Collette, G. Heiman, and J. Xu, "Oscillating bubbles: a versatile tool for lab on a chip applications," Lab Chip **12**(21), 4216–4227 (2012).
2. K. Takahashi, J. G. Weng, and C. L. Tien, "Marangoni effect in microbubble systems," Microsc. Thermophys. Eng. **3**(3), 169–182 (1999).
3. Z. B. Wu and W. R. Hu, "Thermocapillary migration of a planar droplet at moderate and large Marangoni numbers," Acta Mech. **223**(3), 609–626 (2011).
4. J. H. Shin, J. Seo, J. Hong, and S. K. Chung, "Hybrid optothermal and acoustic manipulations of microbubbles for precise and on-demand handling of micro-objects," Sens. Actuators B Chem. **246**, 415–420 (2017).
5. J. Kao, X. Wang, J. Warren, J. Xu, and D. Attinger, "A bubble-powered micro-rotor: conception, manufacturing, assembly and characterization," J. Micromech. Microeng. **17**(12), 2454–2460 (2007).
6. K. Khoshmanesh, A. Almansouri, H. Albloushi, P. Yi, R. Soffe, and K. Kalantar-zadeh, "A multi-functional bubble-based microfluidic system," Sci. Rep. **5**(1), 9942 (2015).
7. K. Takahashi, K. Yoshino, S. Hatano, K. Nagayama, and T. Asano, "Novel applications of thermally controlled microbubble driving system," in Proceedings of IEEE Conference on Micro Electro Mechanical Systems (IEEE, 2001), pp. 286–289.
8. L. Lin, X. Peng, Z. Mao, W. Li, M. N. Yogeesh, B. B. Rajeeva, E. P. Perillo, A. K. Dunn, D. Akinwande, and Y. Zheng, "Bubble-Pen Lithography," Nano Lett. **16**(1), 701–708 (2016).
9. W. C. Nelson and C. Kim, "Droplet actuation by electrowetting-on-dielectric (EWOD): A review," J. Adhes. Sci. Technol. **26**, 1747–1771 (2012).
10. A. Miniewicz, C. Quintard, H. Orlikowska, and S. Bartkiewicz, "On the origin of the driving force in the Marangoni propelled gas bubble trapping mechanism," Phys. Chem. Chem. Phys. **19**(28), 18695–18703 (2017).
11. A. Miniewicz, S. Bartkiewicz, H. Orlikowska, and K. Dradrach, "Marangoni effect visualized in two-dimensions optical tweezers for gas bubbles," Sci. Rep. **6**(1), 34787 (2016).
12. P. Prentice, M. Macdonald, T. Frank, A. Cuschieri, G. Spalding, W. Sibbett, P. Campbell, and K. Dholakia, "Manipulation and filtration of low index particles with holographic Laguerre-Gaussian optical trap arrays," Opt. Express **12**(4), 593–600 (2004).

13. V. Garbin, D. Cojoc, E. Ferrari, R. Z. Proietti, S. Cabrini, and E. Di Fabrizio, "Optical micro-manipulation using Laguerre-Gaussian beams," Jpn. J. Appl. Phys. **44**(7B), 5773–5776 (2005).
14. J. Friend and L. Yeo, "Microscale acoustofluidics: Microfluidics driven via acoustics and ultrasonics," Rev. Mod. Phys. **83**(2), 647–704 (2011).
15. X. Xi, F. B. Cegla, M. Lowe, A. Thiemann, T. Nowak, R. Mettin, F. Holsteyns, and A. Lippert, "Study on the bubble transport mechanism in an acoustic standing wave field," Ultrasonics **51**(8), 1014–1025 (2011).
16. S. Chakraborty, "Electrocapillary," in *Encyclopedia of microfluidics and nanofluidics*, L. Dongqing, ed. (Springer, 2015).
17. X. Qu and H. Qiu, "Bubbles dynamics under a horizontal micro heater array," J. Micromech. Microeng. **19**(9), 095008 (2009).
18. N. A. Ivanova and B. A. Bezuglyi, "Optical thermocapillary bubble trap," Tech. Phys. Lett. **32**(10), 854–856 (2006).
19. O. V. Angelsky, A. Ya. Bekshaev, P. P. Maksimyak, A. P. Maksimyak, S. G. Hanson, and S. M. Kontush, "Controllable generation and manipulation of micro-bubbles in water with absorptive colloid particles by CW laser radiation," Opt. Express **25**(5), 5232–5243 (2017).
20. J. G. Ortega-Mendoza, F. Chávez, P. Zaca-Morán, C. Felipe, G. F. Pérez-Sánchez, G. Beltran-Pérez, O. Goiz, and R. Ramos-Garcia, "Selective photodeposition of zinc nanoparticles on the core of a single-mode optical fiber," Opt. Express **21**(5), 6509–6518 (2013).
21. P. Zaca-Morán, E. Kuzin, J. Torres-Turiján, J. G. Ortega-Mendoza, F. Chávez, G. F. Pérez-Sánchez, and L. C. Gómez-Pavón, "High gain pulsed erbium-doped fiber amplifier for the nonlinear characterization of SWCNTs photodeposited on optical fibers," Opt. Laser Technol. **52**, 15–20 (2013).
22. J. G. Ortega-Mendoza, A. Padilla-Vivanco, C. Toxqui-Quitl, P. Zaca-Morán, D. Villegas-Hernández, and F. Chávez, "Optical fiber sensor based on localized surface plasmon resonance using silver nanoparticles photodeposited on the optical fiber end," Sensors (Basel) **14**(12), 18701–18710 (2014).
23. G. Baffou, J. Polleux, H. Rigneault, and S. Monneret, "Super-heating and micro-bubble generation around plasmonic nanoparticles under cw illumination," J. Phys. Chem. C **118**(9), 4890–4898 (2014).
24. R. Pimentel-Domínguez, J. Hernández-Cordero, and R. Zenit, "Microbubble generation using fiber optic tips coated with nanoparticles," Opt. Express **20**(8), 8732–8740 (2012).
25. M. Kitz, S. Preisser, A. Wetterwald, M. Jaeger, G. N. Thalmann, and M. Frenz, "Vapor bubble generation around gold nano-particles and its application to damaging of cells," Biomed. Opt. Express **2**(2), 291–304 (2011).
26. E. A. Coronado, E. R. Encina, and F. D. Stefani, "Optical properties of metallic nanoparticles: manipulating light, heat and forces at the nanoscale," Nanoscale **3**(10), 4042–4059 (2011).
27. Y. Xie and C. Zhao, "An optothermally generated surface bubble and its applications," Nanoscale **9**(20), 6622–6631 (2017).
28. S. Deguchi, S. Takahashi, H. Hiraki, and S. Tanimura, "Direct measurement of force exerted during single microbubble generation," Appl. Phys. Lett. **102**(8), 084101 (2013).
29. C. E. Brennen, *Cavitation and Bubble Dynamics* (Oxford University, 1999).
30. J. R. Vélez-Cordero and J. Hernández-Cordero, "On the motion of carbon nanotube clusters near optical fiber tips: thermophoresis, radiative pressure and convection effects," Langmuir **31**(36), 10066–10075 (2015).
31. R. S. Subramanian and R. Balasubramanian, *The motion of bubbles and drops in reduced gravity*, (Cambridge University, 2001).
32. J. I. Ramos, "Lumped models of gas bubbles in thermal gradients," Appl. Math. Model. **21**(6), 371–386 (1997).
33. G. Vázquez, E. Alvarez, and J. M. Navaza, "Surface tension of alcohol + water from 20 to 50 °C," J. Chem. Eng. Data **40**(3), 611–614 (1995).
34. L. Parkinson, R. Sedev, D. Fornasiero, and J. Ralston, "The terminal rise velocity of 10-100 μm diameter bubbles in water," J. Colloid Interface Sci. **322**(1), 168–172 (2008).
35. P. H. Jones, E. Stride, and N. Saffari, "Trapping and manipulation of microscopic bubbles with a scanning optical tweezer," Appl. Phys. Lett. **89**(8), 081113 (2006).

1. Introduction

The manipulation of gas and vapor microbubbles inside aqueous solutions has attracted attention because of their applications in the industry as actuators, micro-valves [1,2], manipulation of micro-objects [3,4], development of micro-motors [5,6], ink printers [7], lithography [8], among others. The main mechanism used for the manipulation of microbubbles are based on thermal [9–11], optical [12,13] and acoustic phenomena [14,15]. Thermal techniques based on decrement of surface tension, also called thermocapillary, produce a tangential stress at the vapor-liquid interface called Marangoni force [2,10]. Optical techniques are based in transfer of linear momentum, need a special beam profile produced by beam shaping; while acoustic techniques based on Bjerknes forces employ ultrasonic waves generated by piezoelectric micro-materials [14]. The study of thermal gradients for the generation and migration of microbubbles has been proposed using Joule heating in electrical

devices [16]. X. Qu et al. [17] investigated the dynamics of microbubbles using a horizontal array of electric micro-heaters fabricated using standard micromachining technique. The voltage applied to the array is modulated by a signal generator and amplified for the generation of a thermal gradient. The results showed that the microbubbles can be periodically displaced by the Marangoni force between two heaters separated ~23 μm. By using a laser focused on 50 μm thick cell filled with an absorbing solution, manipulation of microbubbles was also possible without the need of complex microfabrication techniques for the generation of thermal gradients [18]. In this report, the bubbles were already present in the solution with diameters of 0.2-1.2 mm (in fact the bubbles adapted a cylindrical shape) and were attracted towards areas of higher radiation intensity. Recently, Angelsky et al. [19] reported the generation and manipulation of microbubbles based on Marangoni force using a nanocolloidal solution and a cw laser at 980 nm and 2 W of power. Light absorption by the nanoparticles dispersed in water generated a thermal gradient of $\sim 2 \times 10^5$ K m^{-1} resulting in an array of microbubbles with radii up to 130 μm in the beam spot. The array of microbubbles could be manipulated in 2D by displacement of the laser beam.

In this paper, we report the photothermal generation of vapor microbubbles in ethanol due to the radiation absorption from the immobilized silver nanoparticles at the core of an optical fiber. Once the microbubble is created it can be manipulated in 2D and 3D using a low power cw laser at 1064 nm. To the best of our knowledge, generation and manipulation of microbubbles is demonstrated for the first time.

2. Experimental section

In our experimental arrangement, silver nanoparticles (AgNPs) are immobilized on the two multimode optical fibers ends (50/125) using the photodeposition technique [20–22]. A colloidal suspension was made by mixing 0.3 mg of Sigma-Aldrich silver nanopowder (particle size <100 nm) in 2 ml of ethanol, which was mixed in a 4.5 ml capacity polystyrene cuvette. The mixture was homogenized using an ultrasonic bath for 5 minutes. The photodeposition was performed using a IPG Photonics continuous wave laser (CW) model YLR-5-1064-LP that emits at 1064 nm with a maximum power of 240 mW. The laser beam was divided by a 50/50 infrared beam splitter and each beam coupled to the optical fiber terminals using two 10x microscope objectives as shown in Fig. 1.

The photodeposition of the AgNPs on the core of the fibers was carried out by submerging each tip of the optical fiber inside a cuvette filled with a colloidal suspension of alcohol and AgNPs. The rate of photodeposition was monitored using a power meter to achieve an output power of 23 mW (input power 120 mW) corresponding to 7.0 dB attenuation.
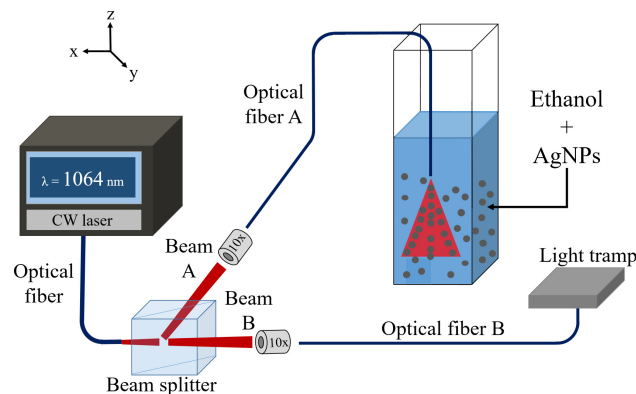

Fig. 1. Experimental setup for photodeposition AgNPs at the core of the optical fibers.

Visualization of the generation and manipulation of microbubbles was performed using a 50x microscope objective with NA = 0.26 and a Phantom high-speed video camera model v7.3 operating at 6600 fps (~151 µs between frames) and illuminated with 12V/20W halogen lamp. The tips of the optical fibers with the photodeposited AgNPs were introduced vertically and horizontally into a cuvette filled with ethanol only as shown in Fig. 2(a) and 2(b) respectively.
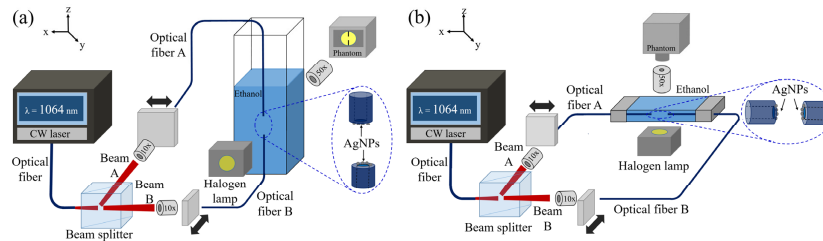

Fig. 2. Experimental setup for the generation and manipulation of microbubbles. (a) Optical fibers vertically opposed. (b) Optical fibers horizontally opposed.

The generation of a microbubble on the fiber tip was carried out by allowing the passage of beam B(A) while beam A(B) is obstructed. The AgNPs deposited at the core of the fiber were heated up by light absorption and then heat is transferred to the surrounding liquid. Depending on the incident power a bubble may be created. Once the bubble is created, beam B(A) is obstructed and beam A(B) is allowed to pass. Thus, the bubble stops growing but maintains its size on the time scale of the experiments. The bubble is affected by the temperature gradient on the opposite fiber tip and is attracted towards it. It should be mentioned that the power used to produce the temperature gradient opposite to the bubble is slightly below (5% less) of that needed for the generation of microbubbles.

3. Experimental results

Figure 3 shows typical snapshots of the microbubble evolution on the tip of the optical fiber considering the experimental setup showed in Fig. 2(a) and laser power of 16 mW. The bubble's radius grows over time due to the continuous ethanol vaporization reaching a radius of 63 µm in 50 ms. The rate of expansion obviously depends on the beam power, however, it should not increase over certain value because cavitation may be produced. The violent collapse of the cavitation bubble may detach the AgNPs until eventually no bubble could be created.
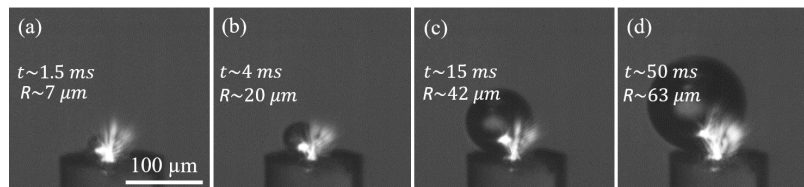

Fig. 3. Sequence of birth (a) and growth of a microbubble (b-d) adhered to the tip of an optical fiber. Bright areas represent scatter light picked up by the camera.

Once the bubble has achieved its desired size, laser beam B(A) is obstructed and beam A(B) is allowed to pass, heating up the other fiber tip. The image sequence shown in Fig. 4 corresponds to vertical ($+z$ direction) displacement of the microbubble between the two tips separated by ~480 µm and where only the beam on the upper fiber is on. It can be observed that the microbubble (115 µm radius) covers the distance in 3.5 ms with a maximum velocity of 238 mm/s while maintaining its spherical shape. It is important to mention that the velocity of the microbubble is not constant and it increases when it approaches the heat source.
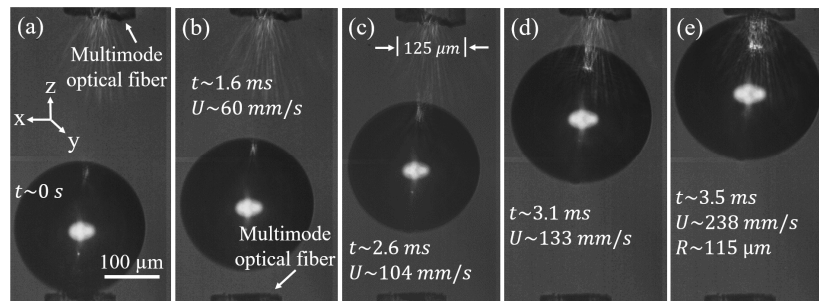
Fig. 4. Snap shots of a travelling microbubble in the + z direction between two opposed optical fibers. The bubble is generated in the lower fiber and attracted towards the upper fiber.

In order to assess the effect of convective currents and buoyancy on the bubble displacement, the bubble was created on the upper fiber and displaced downwards as shown in Fig. 5. The temperature gradient was generated at the lower tip inducing the manipulation of the microbubble in the -z direction. It can be observed that the microbubble (115 μm radius) covers the distance in 5.3 ms with a maximum velocity of 154 mm/s. Note that the downwards velocity is slower than the upwards.
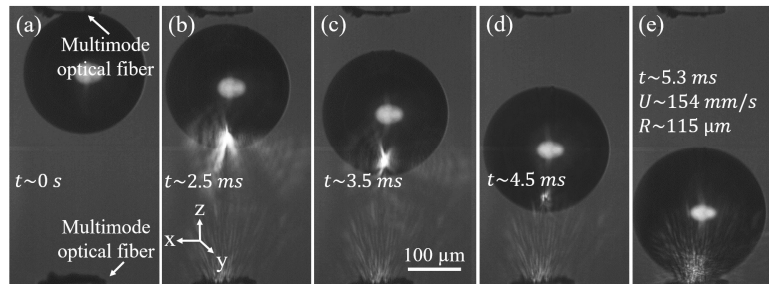

Fig. 5. Snap shots of a travelling microbubble in the -z direction between two opposed optical fibers. The bubble is generated in the upper fiber and attracted towards the lower fiber.

Figure 6(a) shows a frame of Visualization 1 of the periodical manipulation in 2D of a microbubble between two horizontally placed fibers separated by ~1 mm as shown in Fig. 2(b). It is important to note that in this configuration the buoyancy, gravity and drag force do not exist as the height cell is approximately equal to the microbubble size. Furthermore, it can be seen that by switching the position of the temperature gradient it was possible to carry out the horizontal manipulation of a 300 μm radius microbubble (on *y*-axis). It is also possible to manipulate microbubbles when the ends of the fibers are off-axis, as shown in Fig. 6(b) Visualization 2. In the Fig. 6(b) it can be observed that the two fiber tips are spaced 485 μm apart and misaligned 33° with respect to normal. The temperature gradient was generated at the upper tip, producing the upwards displacement (+ z) of the 90 μm radius microbubble. Figure 6(c) shows a frame of Visualization 3 of the manipulation of a microbubble with a radius of 80 μm between two vertically opposed optical fibers, spaced apart 560 μm and misaligned 43° with respect to normal. This time the temperature gradient was generated in the lower fiber, displacing the microbubble in the -z direction, as shown in Visualization 3. Both Visualization 2 and Visualization 3 were record at 6688 fps for 21 ms.
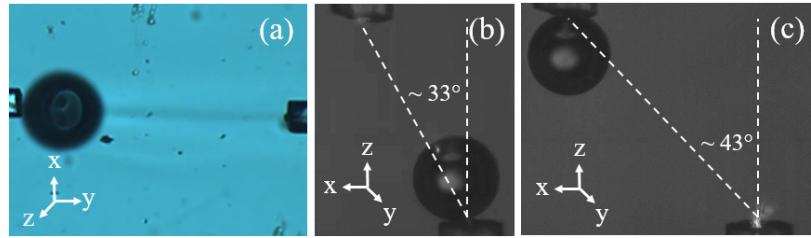
Fig. 6. Manipulation of a microbubble between two horizontally opposed optical fibers (a) due to the switching of the temperature gradients (see Visualization 1). Manipulation of a microbubble in the + z and -z direction between two vertically opposed and off-axis optical fibers (a) 33 ° (see Visualization 2) and (b) 43 ° (see Visualization 3) respectively.

4. Discussion

The results show that microbubbles can be generated by heating due to light absorption at the AgNPs deposited at the fiber end submerged in ethanol [23–25]. Here we show the calculations of the temperature spatial distribution produced by light absorption by the deposited nanoparticles. The steady-state solution for the temperature increase due to a single nanoparticle of radio R in an homogeneous media is given by $\Delta T(r) = \delta_{abs}I/(4\pi\kappa r)$ for $r>R$ where I is the light intensity illuminating the AgNP, δ_{abs} is the absorption cross-section of the AgNP, and κ is the thermal conductivity of the surrounding medium [26]. For a single nanoparticle, the temperature beyond its diameter decays as $1/r$, but for a collection of nonuniform (both in diameter and spatial distribution) or even for uniform closely packed nanoparticles, these temperature decays may be completely different. Thus, calculation and measurements of the temperature profile are difficult to perform given the small dimensions of the volume and time scales involved. However, we can numerically estimate the spatial temperature distribution making reasonable assumptions. First, we simulate the deposited layer as uniform sized nanoparticles having homogenous spatial distribution, so we can assume a uniform temperature distribution and then solve the heat diffusion equation in steady-state coupled to the Navier-Stokes equations using COMSOL Multiphysics. The configuration is quite simple: 50 μm diameter fiber optic is inserted in ethanol and the fiber core-ethanol interface is set to a fixed temperature as shown in Fig. 7. The 2D spatial temperature distribution is shown in Fig. 7(a) and it is possible to observe that this distribution has spherical symmetry while Fig. 7(b) shows the temperature profile along a particular direction r. The continuous line represents the fit to an exponential decay function. Therefore the temperature function in the radial direction is given by:

$$T\left(r\right) = T_0 + \Delta T \exp\left(-\frac{r}{r_D}\right), \tag{1}$$

where T_0 is the ambient temperature, ΔT represents the temperature difference between the fiber core-alcohol interface and ambient temperature, and $r_D \approx 534$ μm represents the heat diffusion length. Although the fitting is not perfect, it can be taken as a good approximation. The achieved temperature depends on the beam power. In order to produce nucleation in ethanol (temperature for vaporization ~78 °C) and therefore bubble formation, a threshold power of 16 mW is needed. In fact, Fig. 3(a) shows the bubble formation obtained with the threshold power. Around time $t = 1.5$ ms the bubble is clearly noticeable. Figure 8 shows the bubble radius dependence on time. The curve fitting was obtained using the equation $R(t) = R_{max}\left(1-\exp\left(-t/\tau_0\right)\right)$ where the maximum bubble radius for this particular power is $R_{max} = 66$ μm and formation time τ_0 is 15 ms. For this reason, it is difficult to obtain bubbles of the same size (< 60 μm) unless a precise control on the opening time is achieved, however,

in our case the control is manual. Previous studies have shown that it is possible to generate microbubbles with low-power continuous-wave lasers in a relative short time [19,27,28].
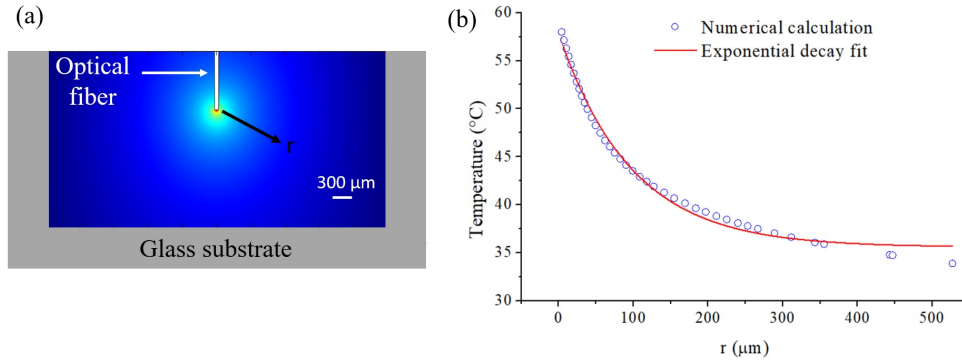
(a)

(b)

Fig. 7. (a) Configuration used to calculate the temperature spatial distribution using COMSOL. The fiber is placed into the cell containing ethanol. (b) Temperature profile from the fiber to the bottom of the cell which in this case r coincides with the z axis.

A microbubble located in the vicinity of the temperature gradient as seen Fig. 7(a) will experience the so called Marangoni force F_M which moves the bubble towards the hot region [29–32]. This force arises by the temperature dependent surface tension differential along the bubble's surface. Due to a tangential stress on the surface tension of the microbubble, the liquid will flow from the lower surface tension (higher temperature) region to the higher surface tension (lower temperature) region as seen Fig. 9. The Marangoni force F_M is given by [29]:

$$\vec{F}_M = -2\pi R^2 \nabla T \frac{d\sigma}{dT},\qquad(2)$$

where R is the radius of the microbubble, ∇T is the temperature gradient in the direction of the radiation source and $d\sigma/dT$ is the temperature derivative of liquid (ethanol) surface tension σ (-0.1×10^{-3} Nm^{-1}K^{-1}) which is practically constant from room temperature up to 70 °C [33].

In addition to the Marangoni force, the microbubble immersed in a liquid also experiences the F_B buoyancy, gravity F_G and drag forces F_D [32,34]. Radiation pressure is negligible given the low power of the beam and the large divergence angle of the light leaving the optical fiber, in addition, light scattering by the nanoparticles contributes to decrease the radiation pressure on the bubble surface [20]. So the buoyancy, gravity and drag forces are given by:

$$\vec{F}_B = \frac{4}{3}\pi \rho_l g R^3,\qquad(3)$$

$$\vec{F}_G = \frac{4}{3}\pi \rho_b g R^3,\qquad(4)$$

$$\vec{F}_D = 6\pi \mu R U,\qquad(5)$$

where g is the gravitational acceleration, U is the velocity of the microbubble, $\mu = 1.071 \times 10^{-3}$ Pa·s is the dynamic viscosity of ethanol, $\rho_l = 789$ kg/m^3 and $\rho_b = 3.4$ kg/m^3 are the density of liquid and the vapor of ethanol, respectively. So, the total force F_T acting on the microbubble traveling between two opposed optically optical fibers is:

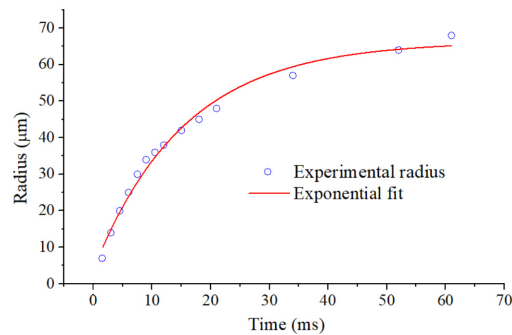$$\vec{F}_T = \vec{F}_B + \vec{F}_D + \vec{F}_G + \vec{F}_M,\qquad(6)$$

Fig. 8. Microbubble radius as function of time.

The direction of the forces involved in the displacement of a microbubble due to the presence of a temperature gradient generated at the top tip of the optical fiber is shown in Fig. 9. The buoyancy force F_B always points upwards while the gravity force F_G always acts downwards. Since the vapor density is two orders of magnitude smaller than the density of liquid, gravity forces will not be taken into account. Marangoni force always is directed to the heat source and its direction can be reversed, as one can observe in Fig. 9.
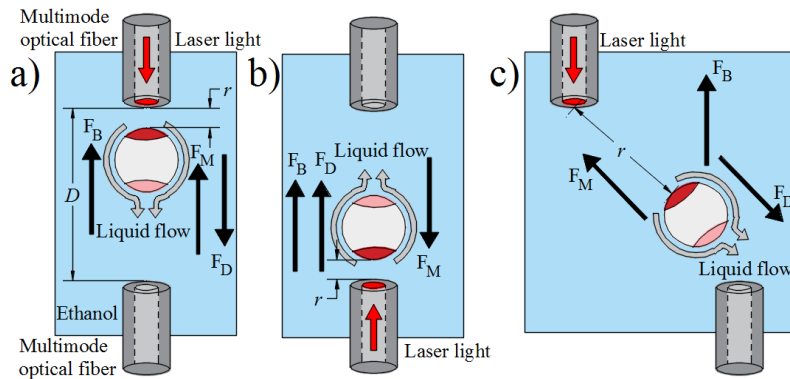

Fig. 9. (a) Displacement of a microbubble in the $+z$ direction, (b) displacement of a microbubble towards $-z$ direction and (c) displacement of microbubble when the optical fibers are off-axis.

Figure 10 shows the Marangoni force and the total force as a function of the distance r between the microbubble and the heat source considering the optical fibers are placed as in Fig. 9(b). In the graph it can be observed that F_M increases when the microbubble approaches the heat source and reaches a magnitude of 400 nN for a 110 μm radius microbubble. Once the bubble reaches the heat source (optical fiber tip) comes to a complete stop. The magnitude of the buoyancy force is 43 nN for a 110 μm radius microbubble. Note that when r is larger than 798 μm, the net force changes sign since buoyancy and drag force overcomes the Marangoni force. The maximum magnitude of Marangoni force for a 110 μm particle radio is one order of magnitude larger than both drag and buoyancy force and is five orders larger than typical gradient optical forces in optical tweezers [35].

The total velocity U of a microbubble immersed in a liquid and under the presence of a temperature gradient is given by:

$$U = U_M + U_T, \tag{7}$$

where U_T is the bubble terminal velocity [34] and U_M is the Marangoni velocity, given by:

$$U_T = \frac{2gR^2}{9\mu}(\rho_b - \rho_l), \tag{8}$$

$$U_M = \frac{d\sigma}{dT}\frac{R}{2\mu r_D}\Delta T \exp\left(-\frac{r}{r_D}\right). \tag{9}$$

Using Eq. (1), Eq. (9) becomes

$$U_M = \frac{d\sigma}{dT}\frac{R}{2\mu r_D}\Delta T \exp\left(-\frac{r}{r_D}\right). \tag{10}$$
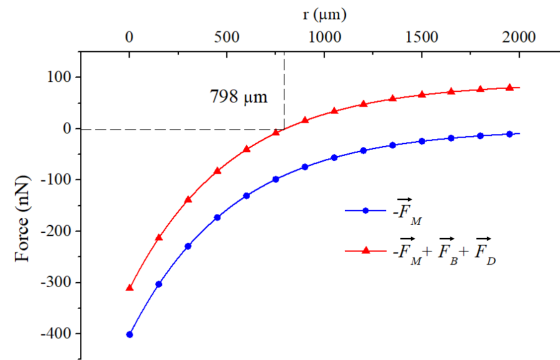

Fig. 10. Marangoni force on a microbubble (with radius $R = 110$ μm, heat source is placed at $r = 0$) as a function of the distance (r) between heat source and the microbubble when the heat source is placed at the lower fiber.

The Marangoni velocity acts in the same direction as the temperature gradient while the terminal velocity always is directed along the $+ z$ direction. For such reason, one should expect a difference in the velocities of the bubble when it moves downwards or upwards as shown in Fig. 11. The results show that for a microbubble of 115 μm radius, the net maximal velocity moving upwards along the z direction reaches 238 mm/s, while the maximal velocity downwards reaches only 155 mm/s. According to Eq. (10), as the bubble approaches the heat source its velocity increases exponentially, which agrees well with experimental measurements shown in Fig. 11(a).

Combining the upwards and downwards velocity bubble we can obtain that $U_T = (U^+ - U^-)/2$ and $U_M = (U^+ + U^-)/2$, where the super indices indicate the direction of the travelling bubble. Calculating the terminal velocity using Eq. (8) one obtains $U_T = 19.65$ mm/s while from experimental data shown in Fig. 11(b), the terminal velocity is ~20 mm/s, which agrees quite well with the theoretical predictions.
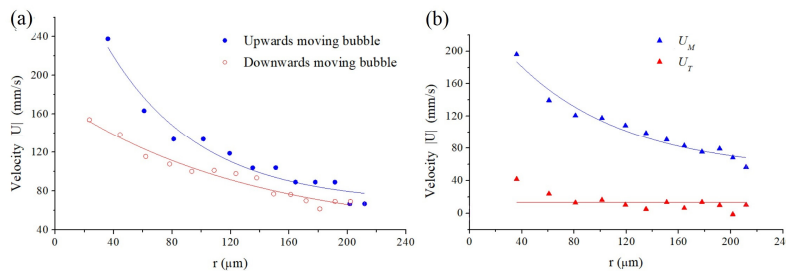

Fig. 11. Microbubble displacement velocity as a function of the distance between the heat source and the microbubble. (a) Dots correspond to experimental data and continuous line corresponds to fittings. (b) Triangles correspond to Marangoni and terminal's velocities as a

result to combining experimental results and continuous lines correspond to fitting of U_M and U_T.

5. Conclusions

It was shown that the generation, 2D and 3D manipulation of microbubbles in a non-absorbent liquid can be carried out through by Marangoni forces activated by light absorption at photodeposited metal NPs on the tip of an optical fiber. Thus, gradient temperature modulates the surface tension of the bubble wall producing a force directed towards the heat source. The temperature gradient allowed the manipulation of microbubbles even when the optical fibers are laterally displaced. Numerical simulations indicate that the temperature gradient is described by an exponential function. Thus, an expression for the Marangoni velocity was obtained. We find that the bubble velocity can be decomposed in two components: constant velocity (terminal velocity) and an accelerated one (Marangoni). Comparison with experiment and theory shows good agreement. The manipulation of a microbubble in 2D and 3D depends on the gradient temperature, microbubble size and the separation distance between the optical fiber tips, whilst in 3D the buoyancy force also is present. The use of optical fibers provides precise spatial control to generate localized temperature gradients; allowing to generate and manipulate microbubbles in areas of difficult access, increasing its accessibility due to the low equipment requirement for its implementation. The generation and manipulation of microbubbles can be used to generate rotary motion in micromotors, directing and controlling flows, transporting particles in MEMS (micro-electro-mechanical-system), among others.